GENERATION OF A NEW HIGH RESOLUTION DDM DATA PRODUCT FROM CYGNSS RAW IF MEASUREMENTS

Hugo Carreno-Luengo[1], Chris Ruf[1], Scott Gleason[2], Anthony Russel[1], and Timothy Butler[1]

[1]Climate and Space Sciences and Engineering Department, University of Michigan (UM)
Ann Arbor, MI, United States of America (USA)
[2]University Corporation for Atmospheric Research (UCAR)
Boulder, CO, United States of America (USA)
Email: {carreno,cruf,russelan,butlerti}@umich.edu, {gleason}@ucar.edu

ABSTRACT

A new CYclone Global Navigation Satellite System (CYGNSS) data product is generated using all the available raw Intermediate Frequency (IF) tracks. In so doing, calibrated Delay Doppler Maps (DDMs) are produced using the CYGNSS raw IF processor, and the CYGNSS End-to-End Simulator (E2ES) to generate Look-Up-Tables (LUTs) to bin-by-bin correct the whole DDMs. Such calibrated DDMs are delivered with shorter incoherent integration time (N_{inc}), finer delay and Doppler resolution, and a wider range of delay and Doppler values as compared to the L1b CYGNSS data product, currently available in the Physical Oceanography Distributed Active Archive Center (PODAAC). This work aims to foster the use of this new data product, so as to improve the performance of CYGNSS for a wide range of scientific applications over land and ocean.

***Index Terms*—** GNSS-R, CYGNSS, raw IF processor, E2ES, DDMs, calibration, data product, scientific applications

1. INTRODUCTION

Global Navigation Satellite Systems Reflectometry (GNSS-R) is a sort of L-band passive multi-bistatic radar, with as many transmitters as navigation spacecrafts are in view e.g. [1-6]. It provides global coverage, full temporal availability, and sampling of the Earth's surface over multiple tracks simultaneously within a wide area up to ~ 1,500 km. Several spaceborne experiments and missions have been deployed. CYGNSS, a NASA's Earth Venture Mission coordinated by the Univervity of Michigan (UM), is the first-ever operational GNSS-R mission [7]. Earth-reflected GNSS signals have sensitivity to a wide variety of geophysical parameters, such Soil Moisture Content (SMC) e.g. [8], Above Ground Biomass (AGB) e.g. [9], and inland water bodies e.g [10].

Raw datasets are collected by CYGNSS. These raw data sets, i.e., the IF signal streams before any receiver processing, can be processed on the ground with the CYGNSS raw IF processor. Each raw dataset consists of one raw IF data file and its metadata file. The raw data file includes three sets of raw signal sample streams (~ 60 s) received by the zenith antenna, and the nadir antennas at port and starboard. The metadata file mainly provides the CYGNSS spacecraft identifier, the instrument, and the timing information.

In this work, we aim to generate a new high resolution calibrated DDM data product from CYGNSS raw IF measurements. This article describes the rationale and the methodology that we are defining so as to generate this new product.

2. THE CYGNSS RAW IF PROCESSOR

The bandwidth of the raw signal is ~ 2.5 MHz, centered at the IF of ~ 3.8 MHz. In the nominal mode, the IF signals are sampled with a sampling rate of ~ 16.0 MHz and a quantizer resolution of 2 bits per sample for both direct and reflected channels.

The CYGNSS raw IF processor [11] can generate full DDMs over the full duration of these CYGNSS raw IF data collections. It uses a delay-domain Fast Fourier Transform (FFT) technique to perform the correlations at all the delay samples using a frequency domain multiplication. The delay sampling is configurable based on decimation of the sampling rate and the Doppler processing range, and the incoherent integration time is completely configurable. The processor runs over the time duration of the entire collection or until it runs out of data.

The CYGNSS raw IF processor was designed and built on a Linux Ubuntu laptop using the free (non-commercial) version of Qt Creator (Version 3.6.0). On Linux, Qt uses the GCC compiler. However, most of the code is written in straight C.

3. ENHANCED DDMs DERIVED FROM CYGNSS RAW IF DATA

The first step was to generate DDMs with high temporal resolution, finer delay and Doppler sampling, and wide delay and Doppler domains (Fig. 1). The reasoning behind the corresponding choices are summarized in the following:

The optimum incoherent integration time N_{inc} was evaluated over several raw tracks when the nominal specular point was in the boundary between land surfaces

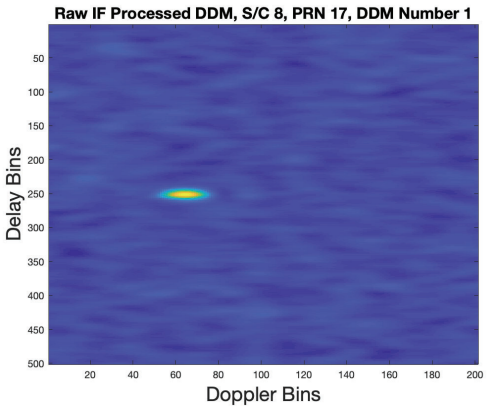


Fig. 1. Sample uncalibrated DDM in raw counts over an inland water body. 1/16 chip delay bin resolution, 32 chips range, 50 Hz Doppler bin resolution, and 10 kHz range.

and lakes. The use of N_{inc} = 40 ms provides the optimum balance between reducing noise by incoherent averaging vs. not smoothing out the rising edge too much (Fig. 2).

The delay chip resolution is determined by the effective sampling rate. In the nominal mode, the raw IF signals are always sampled at the same rate (~ 16 MHz), which is approximately 16,000 samples per mili-second.

Approximately, 16 samples per GPS C/A code chip is a delay chip resolution in the DDM of 1/16 chip. The raw IF processor allows to select other different delay chip resolutions, so that the ~ 16 MHz samples are downsampled:

1/8 chip delay bin resolution: Downsampling by a factor of 2 to get ~ 8 MHz sampling rate or 8 samples per chip.

1/4 chip delay bin resolution: Downsampling by a factor of 4 to get ~ 4 MHz sampling rate or 4 samples per chip.

1/2 chip delay bin resolution: Downsampling by a factor of 8 to get ~ 2 MHz sampling rate or 2 samples per chip, which is the Nyquist limit for the GPS C/A code.

The results were not exactly the same at different delay sampling rates because the processor is taking 1 ms FFTs in each case on different length vectors to perform the correlations (Fig. 2). The shorter the vector the faster the FFT, but delay samples are thrown out. The highest achievable resolution is at the full sampling rate (which has the slowest FFTs), or 16 samples per chip, 1/16 chip delay bin resolution. As such, the use of 1/16 chip delay bin resolution without sample decimation provides the highest fidelity results. The longer run time required is not an important consideration because these data will be archival products that will be stored to be used in the future for the CYGNSS Science Team members.

As the starting point in our work, step sizes for delay and Doppler that are ~ 1/4 the width of the Woodward Ambiguity Function (WAF) in each coordinate were selected. This value oversamples DDMs at roughly twice the Nyquist rate, so there is no loss of any information. The delay and Doppler domains of the new raw IF data product were extended up to 40 Doppler bins x 256 delay bins, so as to generate full DDMs without filteting due to the

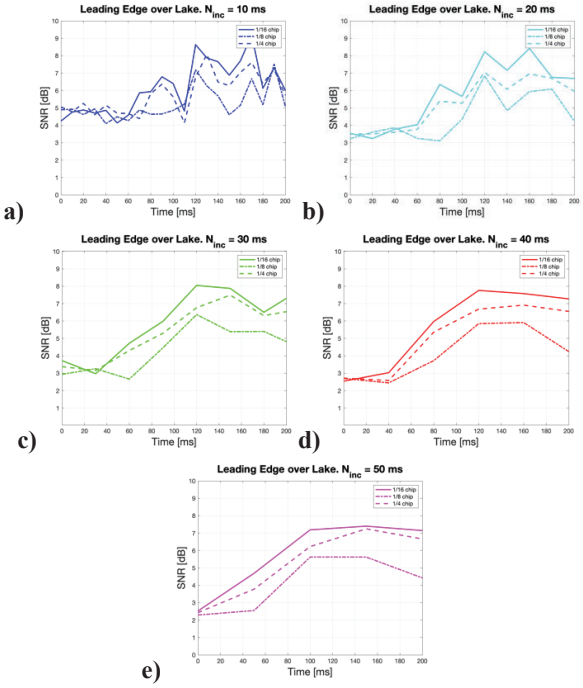


Fig. 2. Evolution of the Signal-to-Noise Ratio (SNR) as the nominal specular point moves from land to a lake surface. The analysis has been performed for 1/16, 1/8, and 1/4 chip delay bin resolution for several incoherent integration times: a) N_{inc} = 10 ms, b) N_{inc} = 20 ms, c) N_{inc} = 30 ms, d) N_{inc} = 40 ms, and e) N_{inc} = 50 ms.

spreading of the trailing edge. This is an improvement as compared to the standard L1 11 x 17 DDMs of the targeted SCI_FULL 20 x 128 DDMs that are currently available on the PODAAC.

4. FULL CYGNSS DDMs CALIBRATION

Raw IF DDMs are generated in raw uncalibrated units. There is a need to generate calibrated DDMs, so as to enable an accurate scientific applicability.

4.1 Calibration Algorithm

The GPS scattered signal power can be expressed as follows:

$$P^{L1a}(\tau, f) = \frac{P_T \lambda^2}{(4\pi)^3} \iint \frac{G_R G_T \sigma^0 |X(\tau, f)|^2}{R_R^2 R_T^2} dA \qquad (1)$$

where P_T is the power of the transmitted signals, $\lambda \sim 19$ cm is the wavelength of the signals, G_T and G_R are the transmitting and receiving antenna gains, R_T and R_R are the ranges from the transmitter and the receiver to the specular point, respectively, X is the WAF, σ^0 is the bistatic scattering coefficient, and τ and f are the delay and Doppler bin.

Equation 1 can be simplified using the effective values of several variables across delay and Doppler bins under the integrand. The effective values include the effect of the

WAF, which are indicated by the over-bar in the following equation [12-14]:

$$P^{L1a}(\tau, f) = \frac{P_T \lambda^2}{(4\pi)^3} \frac{\overline{G_R(\tau, f)} G_T(\tau, f)}{\overline{R_R^2(\tau, f)}\ \overline{R_T^2(\tau, f)}} \langle \sigma^0(\tau, f) \rangle \overline{A(\tau, f)} \quad (2)$$

where $\overline{A(\tau, f)}$ is the effective surface scattering area at each delay/Doppler bin [12-14]:

$$\overline{A(\tau, f)} = \iint |X(\tau, f)|^2 dA \quad (3)$$

The resulting expression for the bin-by-bin scattering cross section is [12-14]:

$$P^{L1b}(\tau, f) = \langle \sigma(\tau, f) \rangle = \frac{P^{L1a}(\tau, f)(4\pi)^3 \overline{R_R^2(\tau, f)}\ \overline{R_T^2(\tau, f)}}{P_T \lambda^2 \overline{G_R(\tau, f)} G_T(\tau, f)} \quad (4)$$

The main difference with respect to the current L1b calibration procedure is on the approximation of eqn. (4). In the generation of the new CYGNSS raw IF data product, no further simplifications are proposed. At present, effective parameters are estimated and applied as constants (corresponding to the nominal specular point) across the DDM measurement, which introduce a certain error away from the nominal specular point.

The standard 11 x 17 DDMs (PODAAC) are calibrated using some approximations that are probably not valid here. For example, DDMs' pixels that do not correspond to the nominal specular point are calibrated using the range to the nominal specular point, since the 11 x 17 DDMs are small enough so that all of the pixels have fairly similar ranges. But with DDMs covering a wider range of delay and Doppler values, this approximation is not valid.

Regarding G_R, the antenna patterns used by the calibration algorithm are tables with 0.1° resolution in elevation and azimuth angles. That is probably sufficient fine so the G_R values used for full DDM calibration can simply be the appropriate table entries.

Regarding the ambiguity in G_R and path loss because two different locations can contribute to the same bin of the full DDM when far away from the nominal specular point, adding a new data field to the full DDM data files, which is an uncertainty DDM, is being considered. It would characterize the effect of this ambiguity on the L1a and L1b calibration algorithms. Along the ambiguity-free line in the full DDM, the uncertainty would be smaller. At bins in the full DDM with the largest difference in G_R and path loss between the two ambiguous contributors, the uncertainty would be larger.

4.2 Calibration Procedure

The CYGNSS E2ES has all the geometry and surface mapping functions to generate bin-by-bin corrections for all the terms that vary over the 11 x 17 DDMs and the 40 x 256 full DDMs. The E2ES was used to generate LUTs to bin-by-bin correct the whole DDMs. These LUTs require some significant computer power, so there is a need to run

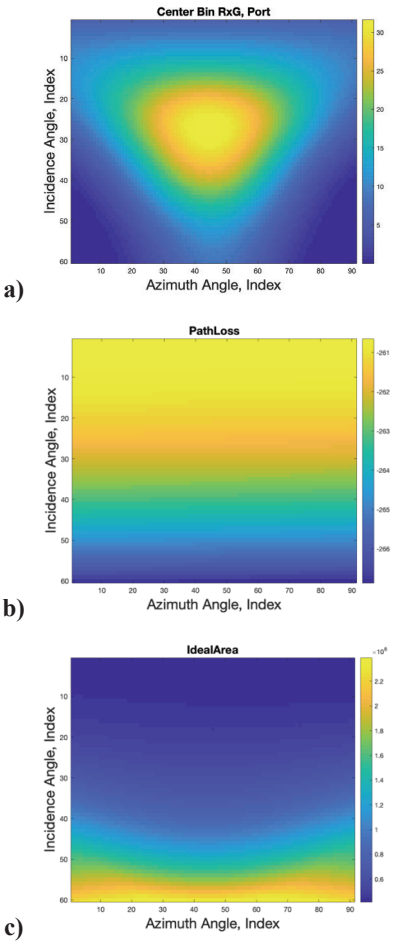


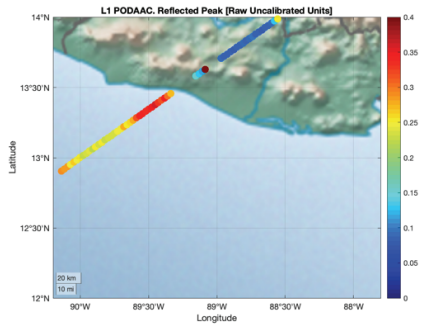
Fig. 3. The calibration procedure maps the near center value in the calibrated DDM over the range of incidence and azimuth angles of the LUT. At each incidence/azimuth point in these plots there is a full DDM which can be used for a bin-by-bin calibration. a) The main lobe of the nadir antenna. b) The path loss. c) The area.

the E2ES at the CYGNSS Science Operation Center (SOC), without disturbing the normal processing. Some first-order approximations are described here:

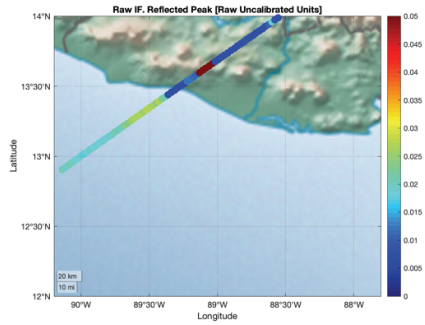
The full DDMs are much larger than the 11 x 17 surface area. So, as the E2ES performs a surface integration, the E2ES quickly overwhelm in generating larger LUTs. The LUTs needs to be a function of elevation and azimuth, for both port and starboard. However, the E2ES can generate LUTs for most of the above parameters (even effective ones). The most critical issue is how big a surface must be to make it integrate over, and at what spatial step. As a starting point, the mapping of G_T was skipped because the path loss and G_R have a much larger impact.

LUTs were generated for a nominal attitude, without pointing errors. Adding an additional roll dimension into the LUTs is under our considerations.

The calibration procedure maps the near center value in the calibrated DDMs over the range of incidence and azimuth angles of the LUT. At each incidence/azimuth point in Fig. 3 there is a full DDM which can be used for a



a)



b)

Fig. 4. Normalized reflected peak-power [raw uncalibrated units] over one-sample CYGNSS track: a) L1 PODAAC, b) raw IF processor.

bin-by-bin calibration. The main lobe of the nadir antenna is shown in Fig. 3a. Fig. 3b shows that the path loss is constant across azimuth and increases with incidence angle. Finally Fig. 3c shows that the area behavior is similar. This is only needed to attempt Normalized Bistatic Radar Cross-Section (NBRCS) values over regions of the DDMs.

4.3 Comparison PODAAC-derived vs. Raw IF Uncalibrated DDMs

As a starting point, several raw IF tracks have been seleted and the corresponding 11 x 17 DDMs have been generated from it with 500 ms incoherent integration time, 1/4 chip delay bin resolution, and 500 Hz Doppler bin resolution. These DDMs were compated to the raw counts DDMs from PODAAC (Fig. 4), so as to generate a scale factor between both types of uncalibrated DDMs. This scale factor (Fig. 5) is being applied to the raw IF DDMs so as to produce intercomparable results. Finally, E2ES-derived LUTs will be applied to these raw IF DDMs and results will be compared to the calibrated DDMs from PODAAC.

5. CONCLUSIONS

We are working in several tasks so as to generate a new high resolution calibrated DDM data product from CYGNSS raw IF measurements. This new product aims to improve the performance of CYGNSS for a wide range of scientific studies over land and ocean.

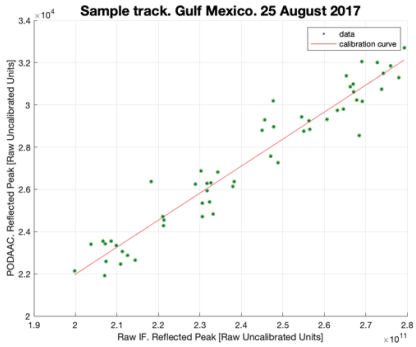


Fig. 5. Scale factor between reflected peak-power [raw uncalibrated units] times series from PODAAC and the raw IF processor.

5. REFERENCES

[1] M. Martin-Neira, "A Passive Reflectometry and Interferometry System (PARIS): Application to Ocean Altimetry," ESA Journal, vol. 17, no. 9, pp. 331-355, 1993.
[2] V.U. Zavorotny and A.G. Voronovich, "Scattering of GPS Signals from the Ocean with Wind Remote Sensing Application," IEEE Transactions on Geoscience and Remote Sensing, vol. 38, no. 2, pp. 951-964, Mar. 2000.
[3] J.L. Garrison, A. Komjathy, V.U. Zavorotny, and S.J. Katzberg, "Wind Speed Measurement Using Forward Scattered GPS Signals," IEEE Transactions on Geoscience and Remote Sensing, vol. 40, no. 1, pp. 50-65, 2002.
[4] S.T. Lowe, J.L. LaBrecque, C. Zuffada, L.J. Romans, L.E. Young, and G.A. Hajj, "First Spaceborne Observation of an Earth-Reflected GPS Signal," Radio Science, vol. 37, pp. 7-1–7-28, 2002.
[5] S. Gleason, S. Hodgart, Y. Sun, C. Gommenginger, S. Mackin, M. Adjrad, and M. Unwin, "Detection and Processing of Bistatically Reflected GPS Signals from a Low Earth Orbit for the Purpose of Ocean Remote Sensing," IEEE Transactions on Geoscience and Remote Sensing, vol. 43, no. 6, pp. 1229-1241, 2005.
[6] K.M. Larson, E.E. Small, E. Gutmann, A. Bilich, P. Axelrad, and J. Braun, "Using GPS Multipath to Measure Soil Moisture Fluctuations: Initial Results," GPS Solutions, vol. 12, no. 3, pp. 173-177, 2008.
[7] C.S. Ruf, R. Atlas, P.S. Chang, M.P. Clarizia, J.L. Garrison, S. Gleason, S.J. Katzberg, Z. Jelenak, J.T. Johnson, S.J. Majumdar, A. O'brien, D.J. Posselt, A.J. Ridley, R.J. Rose, and V.U. Zavorotny, "New Ocean Winds Satellite Mission to Probe Hurricanes and Tropical Convection," Bulleting American Meteorological Society, vol. 97, pp. 385-395, 2015.
[8] H. Carreno-Luengo, S.T. Lowe, C. Zuffada, S. Esterhuizen, and S. Oveisgharan, "Spaceborne GNSS-R from the SMAP Mission: First Assessment of Polarimetric Scatterometry over Land and Cryosphere," MDPI Remote Sensing, vol. 9, pp. 362, 2017.
[9] H. Carreno-Luengo, G. Luzi, and M. Crosetto, "Above-Ground Biomass Retrieval over Tropical Forests: A Novel GNSS-R Approach with CYGNSS," MDPI Remote Sensing, vol. 12, no. 9, pp. 1368, 2020.
[10] C. Gerlein-Safdi, and C. Ruf, "A CYGNSS-Based Algorithm for the Detection of Inland Waterbodies," Geophysical Research Letters, vol. 46, no. 21, pp. 12065-12072, 2019.
[11] S. Gleason, "CYGNSS DDM Processor Basics," 2017.
[12] S. Gleason, "Algorithm Theoretical Basis Document Level 1B DDM Calibration," CYGNSS Project Document 148-0137, Rev. 2, 2018.
[13] S. Gleason, C.S. Ruf, M.P. Clarizia, and A.J. O'Brien, "Calibration and Unwrapping of the Normalized Scattering Cross Section for the Cyclone Global Navigation Satellite System," IEEE Journal of Selected Topics in Applied Earth Observations and Remote Sensing, vol. 54, no. 5, pp. 2495-2509, 2016.
[14] S. Gleason, C.S. Ruf, A.J. O'Brien, and D.S. McKague, "The CYGNSS Level 1 Calibration Algorithm and Error Analysis Based on On-Orbit Measurements," IEEE Journal of Selected Topics in Applied Earth Observations and Remote Sensing, vol. 12, no. 1, pp. 37-49, 2019.

Acknowledgements

This research was supported in part by the NASA Science Mission Directorate contract NNL13AQ00C with the University of Michigan.